Carbohydrate Polymers 81 (2010) 409–419

Contents lists available at ScienceDirect

Carbohydrate Polymers

journal homepage: www.elsevier.com/locate/carbpol

Enhanced entrapment efficiency and modulated drug release of alginate beads loaded with drug–clay intercalated complexes as microreservoirs

Thaned Pongjanyakul*, Thitiphorn Rongthong

Faculty of Pharmaceutical Sciences, Khon Kaen University, 123 Mittraphap Road, Khon Kaen 40002, Thailand

ARTICLE INFO

Article history:
Received 28 January 2010
Received in revised form 16 February 2010
Accepted 22 February 2010
Available online 6 March 2010

Keywords:
Alginate bead
Propranolol
Magnesium aluminum silicate
Complexes
Drug entrapment efficiency
Drug release

ABSTRACT

Calcium alginate (CA) beads loaded with intercalated complexes of propranolol HCl (PPN) and magnesium aluminum silicate (MAS), which serve as microreservoirs, were prepared using an ionotropic gelation method. The surface and matrix morphology, drug entrapment efficiency, thermal behavior, mechanical properties, and PPN release of the CA beads were characterized. The results showed that the molecular interaction of MAS with PPN and sodium alginate (SA) resulted in PPN–MAS intercalated complex particles as microservoirs and denser matrix structure formation in the CA beads. The small particles of the PPN–MAS complexes were embedded on the surface and in the matrix of the CA beads, which was revealed using SEM and EDX. The PPN entrapment efficiency of the PPN–MAS complex-loaded CA beads was significantly higher than that of the PPN-loaded CA beads. Increased MAS content caused an increase in PPN entrapment efficiency, thermal stability, and the strength of the CA beads. Moreover, the PPN–MAS complexes in the CA beads could remarkably reduce the initial burst of PPN release as well as its release rate in both 0.1 M HCl and phosphate buffer at pH 6.8, depending on the MAS content added. Additionally, the PPN–MAS complex-loaded CA beads also produced a sustained release pattern of PPN in simulated gastro-intestinal conditions. In conclusion, the CA beads containing drug–clay intercalated complexes as microreservoirs could enhance drug entrapment efficiency, reduce initial burst release and modulate drug release. Furthermore, these beads represent a promising oral drug delivery system for highly water-soluble cationic drugs.

1. Introduction

In oral drug delivery systems, the dosing of drugs in multiple-units has been found to have advantages over single-unit dosage forms (Bechgaard & Nielsen, 1978). Multiple-unit dosage forms are often composed of numerous particles that are contained in a tablet or a capsule. The small particles are mixed with the contents of the gastro-intestinal (GI) tract and are distributed over a large area. Therefore, high local concentrations of the drug are avoided, and the risk of local irritations is reduced. Additionally, multiple-units are less variable and less dependent on gastric transit time, which results in a reproducible bioavailability of the drug.

Small beads have been used as drug carriers to prepare oral multiple-unit capsules intended for sustained release dosage forms (Takada & Yoshikawa, 1999). These beads can be prepared using an ionotropic gelation method, where polysaccharides are cross-linked to form an insoluble gel bead. Sodium alginate (SA), which is a naturally occurring non-toxic polysaccharide found in marine brown algae, is one of the polysaccharides employed to fabricate small beads. Gelation of SA occurs when uronic acids (α-L-guluronic and β-D-mannuronic acids) are cross-linked with divalent cations, such as calcium ions (Draget, 2000). Gelation occurs when the extended chain sequences of these acids adopt a regular twofold conformation and dimerize by chelating calcium, forming the so-called 'egg-box' structure (Grant, Morris, Rees, Smith, & Thom, 1973). Each calcium ion takes part in nine coordination bonds with each oxygen atom, resulting in a three-dimensional network of calcium alginate (CA). This phenomenon has been applied to the preparation of CA beads for use as a drug delivery system, by dropping the drug-containing SA dispersion into a calcium chloride bath (Østberg, Lund, & Graffner, 1994; Sugawara, Imai, & Otagiri, 1994). The CA beads could protect an acid-sensitive drug from gastric juice, and the drug was consequently released from the beads in the intestine (Fernández-Hervás, Holgado, Fini, & Fell, 1998; Hwang, Rhee, Lee, Oh, & Kim, 1995).

A low entrapment efficiency of water-soluble drugs in the CA beads is a problem for developing CA beads as a drug delivery system (Lee, Min, & Cui, 1999). This is largely due to the leakage of drug molecules from the wet beads during the cross-linking process. To solve this problem, the incorporation of water-soluble polymers, such as chondroitin sulfate (Murata, Miyamoto, & Kawashima, 1996), konjac glucomannan (Wang & He, 2002), gelatin (Almeida

* Corresponding author. Tel.: +66 43 362092; fax: +66 43 202379.
E-mail address: thaned@kku.ac.th (T. Pongjanyakul).

0144-8617/$ – see front matter © 2010 Elsevier Ltd. All rights reserved.
doi:10.1016/j.carbpol.2010.02.038

& Almeida, 2004), sodium starch glycolate (Puttipipatkhachorn, Pongjanyakul, & Priprem, 2005), and xanthan gum (Pongjanyakul & Puttipipatkhachorn, 2007a), have been used to improve drug entrapment efficiency by reinforcing CA beads due to complex formation of SA with such water-soluble polymers. An alternative approach involves the use of water insoluble materials for reinforcement of the CA beads. Due to the formation of a complex between the carboxyl groups of SA and the amino groups of chitin, water insoluble chitin has previously been added to the beads to retard drug release (Murata, Tsumoto, Kofuji, & Kawashima, 2003). Furthermore, complexes formed between an amine drug and a synthetic cation exchange resin have been applied as a drug carrier in the CA beads (Halder, Maiti, & Sa, 2005).

Magnesium aluminum silicate (MAS) is a mixture of natural smectite clays, specifically montmorillonite and saponite (Kibbe, 2000; Viseras, Aguzzi, Cerezo, & Lopez-Galindo, 2007). MAS has a layered silicate structure, and the surface of the silicate layer contains numerous silanol groups (SiOH), which are able to form hydrogen bonds with other substances (Gupta, Vanwert, & Bogner, 2003). The separation of the layered structures occurs when these clays are hydrated in water, and the weakly positively charged edges and the negatively charged faces of MAS are presented. Due to the interaction of the silanol groups of MAS with the carboxyl groups of SA, MAS has been used to improve the physical properties of CA beads (Puttipipatkhachorn et al., 2005). Recently, MAS was used as an adsorbent for amine drugs to form drug-MAS complexes. A simultaneous formation of small particle drug-MAS complexes occurred when a MAS dispersion and a drug solution were mixed, due to electrostatic interactions between these materials (Rojtanatanya & Pongjanyakul, 2010; Suksri & Pongjanyakul, 2008). Thus, the drug-MAS complexes obtained provided a sustained release pattern of the drug (Pongjanyakul, Khunawattanakul, & Puttipipatkhachorn, 2009; Rojtanatanya & Pongjanyakul, 2010). Therefore, it is possible that the drug-MAS complexes can be added to a SA dispersion before the cross-linking process to prepare CA beads that contain drug-MAS complexes, which serve as drug microreservoirs. The resulting complexes may enhance drug entrapment efficiency and modulate drug release.

Propranolol HCl (PPN), a secondary amine compound with high water solubility, was the first β-adrenoceptor-blocking drug to achieve wide therapeutic use for the treatment of angina and hypertension (Dollery, 1991). Due to the short half-life of PPN (3.9 h) (Dollery, 1991), PPN has been selected as a drug candidate for developing multiple-unit sustained release dosage forms (Paker-Leggs & Neau, 2009). Moreover, PPN has previously been reported to form small particle complexes with MAS (Rojtanatanya & Pongjanyakul, 2010). Therefore, the aim of this study was to prepare and investigate CA beads loaded with PPN–MAS complexes that serve as microreservoirs. The SA dispersions containing PPN–MAS complexes formed with different MAS concentrations were prepared and characterized according to particle size, zeta potential, and the amount of PPN adsorbed prior to cross-linking using different concentrations of calcium chloride. The surface and matrix morphology of the PPN–MAS complex-loaded CA beads were investigated using a scanning electron microscopy and energy dispersive X-ray analysis. Moreover, PPN entrapment efficiency, thermal behavior, mechanical properties, and PPN release of the beads were examined.

2. Materials and methods

2.1. Materials

MAS (Veegum®HV, Lot No. V-GHV-5H-367) and PPN (Batch No. M080115) were purchased from the R.T. Vanderbilt Company, Inc. (Norwalk, CT, USA) and Changzhou Yabang Pharmaceutical Co., Ltd. (Jiangsu, China), respectively. SA (Manugel®DMF, Batch No. 991131) was obtained from ISP Thailand Ltd. (Bangkok, Thailand). All other reagents used were of analytical grade and used as received.

2.2. Preparation of PPN–MAS complex dispersions

A 4% (w/v) MAS suspension was prepared using hot water and cooled to room temperature prior to use. Next, the 4% (w/v) MAS suspension in 4.7, 9.4 or 18.8-ml volumes were mixed with 25 ml of the 1% w/v PPN deionized water solution in a beaker, and then the PPN–MAS dispersions were adjusted to a final volume of 50 ml to yield MAS concentrations of 0.38, 0.75, or 1.5% (w/v), respectively. The pH of all dispersions was approximately 7.6, which was measured using a pH meter (Ion Analyzer 250, Corning, USA). Next, the dispersions were incubated at 25 °C for 24 h to allow PPN adsorption onto the MAS particles to equilibrate and obtain complete formation of the PPN–MAS complexes. The PPN–MAS complex dispersions were investigated as described in Section 2.4.

2.3. Preparation of SA dispersions with PPN–MAS complexes

SA (0.75 g) was gently added to the PPN–MAS complex dispersions, which had been incubated at 25 °C for 24 h. The SA dispersions with PPN–MAS complexes were incubated again at 25 °C for 24 h. Then, the dispersions obtained were characterized and used to prepare the CA beads.

2.4. Characterization of PPN–MAS complex dispersions

2.4.1. Microscopic morphology studies

The morphology of the PPN–MAS complexes in the dispersions was investigated using an inverted microscope (Eclipse TS100, Nikon, Japan) and imaged using a digital camera (Coolpix 4500, Nikon, Japan).

2.4.2. Particle size determination

The sizes of the MAS particles and the PPN–MAS complexes in the dispersions were measured using a laser diffraction particle size analyzer (Mastersizer2000 Model Hydro2000SM, Malvern Instrument Ltd., UK). The samples were dispersed in 70 ml of deionized water in a small volume sample dispersion unit and stirred at a rate of 50 Hz for 30 s prior to measurement. The particle sizes in terms of volume weighted mean diameter were then recorded.

2.4.3. Zeta potential measurement

The zeta potential of the MAS particles and the PPN–MAS complexes in the dispersions were measured using a laser Doppler electrophoresis analyzer (Zetasizer Model ZEN 2600, Malvern Instrument Ltd., UK). The samples were kept at 25 °C, and the dispersions were diluted using deionized water to obtain the appropriate concentrations (count rates >20,000 counts per second) prior to measurement.

2.4.4. Determination of PPN adsorbed onto MAS

The clear supernatants of the dispersions were collected, diluted with deionized water, and then filtered through a 0.45-μm cellulose acetate membrane. The amount of PPN in the supernatants was analyzed using an UV–vis spectrophotometer (Shimadzu UV1201, Japan) at a wavelength of 289 nm. The amount of PPN adsorbed onto the MAS was calculated as the difference between the amount of PPN added and the amount of PPN in the supernatant.

2.4.5. Rheological studies of composite dispersions

Rheological properties and viscosity of the dispersions were studied using a small sample adapter of a Brookfield Digital Rheometer (Model DV-III, Brookfield Engineering Labs Inc., Stoughton, MA) at 32 ± 1 °C. A rheogram of the samples was obtained by plotting the shear rate and the shear stress from various revolution rates when a spindle (no. 34) was used. To characterize the type of flow of the samples, the following exponential formula was used (Martin, 1993):

$$F^N = \eta G \quad (1)$$

$$\text{Log } G = N \text{ Log } F - \text{Log } \eta \quad (2)$$

where G, F, N and η are shear rate, shear stress, exponential constant that defines the type of flow, and viscosity coefficient, respectively. The N value is approximately unity, indicating Newtonian flow, whereas increasing of the N value more than unity represents pseudoplastic flow of the dispersions.

2.5. Preparation of beads

PPN–MAS complex-loaded CA beads were prepared by dropping the SA dispersions containing PPN–MAS complexes that were prepared in Section 2.3 through a nozzle (1.2 mm inner diameter) into 0.5, 1.0, or 2.0% (w/v) calcium chloride solution (80 ml) with gentle agitation. The gel beads were cured in this solution for 30 min, washed 2 times with 20 ml of deionized water, blotted to remove excess water, and dried at 50 °C for 24 h. To prepare blank beads and PPN-loaded CA beads, the 1.5% SA dispersions without and with 0.5% PPN, respectively, were prepared, and bead preparation proceeded as described above.

2.6. Characterization of beads

2.6.1. Particle size analysis

The particle size of the beads was determined using an optical microscope (Nikon, Japan). One hundred beads were randomly selected, and their Feret diameters were measured.

2.6.2. Determination of drug entrapment efficiency

The beads were ground using a mortar and pestle, and 100 mg of the ground beads was dispersed in 50 ml of 2 M HCl. The mixture was sonicated for 30 min and incubated at 37 °C for 24 h. The solution was then filtered, and the PPN content was assayed using an UV–vis spectrophotometer (Shimadzu UV1201, Kyoto, Japan) at a wavelength of 289 nm. The entrapment efficiency was calculated according to the ratio of actual to the theoretical drug content in the beads (Wang & He, 2002).

2.6.3. Scanning electron microscopy (SEM) with energy dispersive X-ray (EDX) analysis

The surface and matrix morphology of the beads were observed using scanning electron microscopy (SEM). The samples were mounted onto stubs, which were then sputter coated with gold in a vacuum evaporator and photographed using a scanning electron microscope (Jeol Model JSM-6400, Tokyo, Japan). Additionally, the surface chemical analysis of the samples was investigated by EDX analysis (Link ISIS series 300, Oxford Instruments, England). The characteristic X-rays emitted and elemental information of the samples were recorded.

2.6.4. Differential scanning calorimetry (DSC)

DSC thermograms of the samples were recorded using a differential scanning calorimeter (DSC822, Mettler Toledo, Switzerland). Each sample (2.0–2.5 mg) was accurately weighed into a 40-μl aluminum pan without a cover. The measurements were performed over 30–450 °C, heating at a rate of 10 °C min^{-1}.

2.6.5. Fourier transform infrared (FTIR) spectroscopy

FTIR spectra of the samples in KBr discs were recorded with a FTIR spectrophotometer (Spectrum One, Perkin Elmer, Norwalk, CT). Each sample was gently triturated with KBr powder at a weight ratio of 1:100 and then compacted into a disc using a hydrostatic press at 10 tons for 5 min. The disc was placed in the sample holder and scanned from 4000 to 450 cm^{-1} at a resolution of 4 cm^{-1}.

2.6.6. Mechanical property of beads

The method for determining the mechanical property of the beads was modified from a previous reported by Edwards-Lévy and Lévy (1999). Analysis of the mechanical property of the beads was carried out using a texture analyzer (TA.XT plus, Stable Micro Systems, UK) with a 50-kg load cell equipped with a cylindrical probe of 6 mm in diameter. One bead was placed on the platform at room temperature. The probe was positioned to touch the bead, recorded as the initial position, and then the probe flattened the bead at a constant speed of 1.0 mm s^{-1}. The probe was removed when the bead was reduced to 50% of its original height. The force and percent displacement was plotted, and the maximum force at 50% displacement, which represents the strength of the beads, was reported.

2.6.7. In vitro drug release studies

A USP dissolution apparatus I (Hanson Research, Northridge, CA) was used to characterize the release of PPN from the beads. The baskets were rotated at a rate of 50 rev. min^{-1} at 37.0 ± 0.5 °C. The amount of beads added to 500 ml dissolution medium was equivalent to 20 mg of PPN. The dissolution media used were 0.1 M HCl and pH 6.8 phosphate buffer. The simulated gastro-intestinal conditions used to measure drug release were performed using 0.1 M HCl (500 ml) for 2 h, followed by pH 6.8 phosphate buffer (500 ml). Samples (20 ml) were collected and replaced with fresh media at various time intervals. The amount of PPN released was analyzed spectrophotometrically at 289 nm (Shimadzu UV1201, Japan).

The PPN release kinetics from the CA beads in various dissolution media were investigated by fitting the PPN release data into zero order and Higuchi's models, which can be expressed using the following equation:

$$Q = kt^n \quad (3)$$

Here, Q is the percentage of drug released at a given time (t), k is the release rate and n is the diffusion exponent. The n value could be defined as 0.5 and 1, which indicated the Higuchi's and zero order equation, respectively (Costa & Lobo, 2001). The release rate was estimated by fitting the experimental drug release data into both models and analyzed by linear regression analysis.

3. Results and discussion

3.1. Characteristics of PPN–MAS complexes

The PPN solution was mixed with different concentrations of MAS to form the flocculates or complexes, as shown in Fig. 1a. This phenomenon occurred due to the molecular interaction between the negatively charged MAS and cationic PPN (Rojtanatanya & Pongjanyakul, 2010). The characteristics of the PPN–MAS complex dispersions are presented in Table 1. The MAS particle size was 4.81 ± 0.17 μm, whereas the mean particle sizes of the PPN–MAS complexes ranged from 65.9 to 75.9 μm. The zeta potential of the negatively charged complexes and the percentage of PPN adsorbed onto MAS increased with increasing MAS concentration. This was

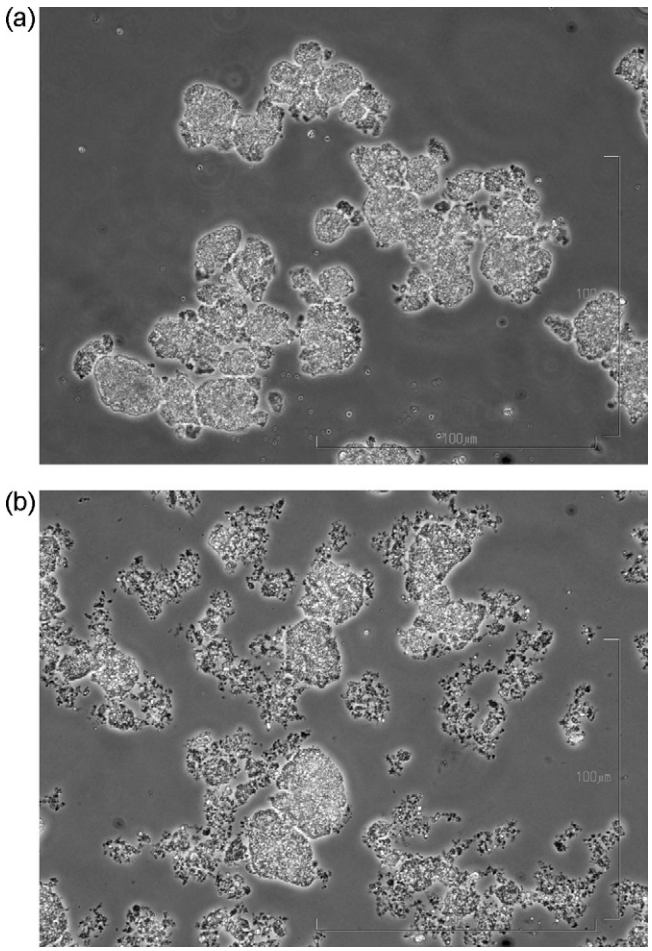

Fig. 1. Microscopic morphology of PPN–MAS complexes in distilled water without (a) and with 1.5% (w/v) SA (b).

because a fixed concentration of PPN was used in the dispersions and the increased MAS provided additional negative charges and higher adsorption sites for PPN. The incorporation of SA into the PPN–MAS dispersions resulted in PPN–MAS complexes with smaller particle sizes and a higher percentage of PPN adsorbed onto the MAS (Table 1). An explanation for the smaller particle sizes is shown in Fig. 1b. Specifically, the PPN–MAS complexes were broken into smaller particles because the negative charge of SA could interact molecularly not only with MAS (Pongjanyakul & Puttipipatkhachorn, 2007b) but also with the positive charge of PPN. However, the smaller particle sizes of the PPN–MAS complexes possessed a larger surface area for PPN adsorption, and therefore a higher percent of PPN was adsorbed.

The rheology of the 1.5% SA dispersion was Newtonian, with an N value close to 1 (Table 1). The presence of PPN in the SA dispersion increased the viscosity coefficient. This is likely due to the partially electrostatic interaction of the negatively charged SA with the cationic drug (Bertram & Bodmeier, 2006). The presence of MAS in the dispersions seemed to increase the N value and the viscosity coefficient of the dispersions. The PPN–1.5% MAS dispersion with SA had the highest *N* value and viscosity coefficient, indicating that the interaction between MAS and SA could change the rheological behavior from Newtonian to pseudoplastic flow and could increase the viscosity of the dispersion in a manner similar to previous studies (Pongjanyakul & Puttipipatkhachorn, 2007b). This finding suggested that the formation of the PPN–MAS complexes and the increase in viscosity of the dispersions might affect the cross-linking process of the alginate beads in the calcium chloride solution.

3.2. FTIR studies

The molecular interactions of SA, PPN and MAS in the CA beads were investigated using FTIR spectroscopy. FTIR spectra of SA powder showed peaks around 3435, 1615, 1418, and 1031 cm^{-1}, reflective of O–H, COO^- (asymmetric), COO^- (symmetric), and C–O–C stretching, respectively (Pongjanyakul & Puttipipatkhachorn, 2007a). The cross-linking process of SA with calcium caused an obvious shift to higher wave numbers and a decrease in the intensity of COO^- stretching peaks. Additionally, a change to lower wave numbers and a decrease in the intensity of the C–O–C stretching peak of SA was observed (Fig. 2c). This indicated the presence of an ionic bond between the calcium ion and the carboxyl groups of SA and partial covalent bonding between the calcium and oxygen atoms of the ether groups, and it is in agreement with previous studies (Sartori, Finch, & Ralph, 1997). The PPN-loaded CA beads caused a shift in the O–H, COO^- (asymmetric), and COO^- (symmetric) stretching peaks to lower wave numbers, suggesting that a molecular interaction between SA and PPN was formed due to hydrogen bonding and electrostatic force. Furthermore, these results suggest that this interaction occurred before the cross-linking process, which is in agreement with a previous study (Lim & Wan, 1997). This finding can account for the changes in the rheological properties of the SA dispersion with PPN. The addition of MAS in the PPN-loaded CA beads caused a change in the carboxylate peaks of SA. The Si–O–Si stretching peak of MAS at 1015 cm^{-1} (Fig. 2b) became narrower and moved to a lower wave number (Fig. 2e), suggesting that MAS could interact with SA and PPN in the beads. Moreover, the PPN peaks at 775, 797, 1241 and 1270 cm^{-1} were found in the spectra of the PPN–1.5% MAS complex-loaded CA beads and were not observed in the spectra of PPN-loaded CA beads. These results suggested that the PPN–MAS complex-loaded CA beads might have a higher PPN entrapment efficiency.

Table 1
Characteristics of PPN–MAS complexes and SA dispersions with PPN–MAS complexes.

Dispersion	Particle size (μm)	Zeta potential (mV)	PPN adsorbed (%)	*N*	Viscosity coefficient ([dyne cm^{-2}]^N s)
0.5% PPN–MAS dispersion					
−0.38% MAS	75.9 ± 2.3	−6.2 ± 0.5	15.0 ± 1.6	–	–
−0.75% MAS	65.9 ± 2.6	−18.5 ± 2.6	34.5 ± 0.6	–	–
−1.50% MAS	66.1 ± 1.5	−26.2 ± 1.4	69.9 ± 0.4	–	–
1.5% SA dispersion	–	–	–	0.98 ± 0.01	5.23 ± 0.22
+0.5% PPN	–	–	–	1.04 ± 0.01	8.23 ± 0.29
+0.5%PPN–MAS					
−0.38% MAS	15.6 ± 0.3	−77.2 ± 2.9	27.9 ± 3.2	1.06 ± 0.01	11.64 ± 0.38
−0.75% MAS	23.9 ± 0.5	−90.1 ± 2.4	47.3 ± 0.4	1.06 ± 0.02	11.35 ± 1.07
−1.50% MAS	54.7 ± 1.2	−93.6 ± 2.9	77.4 ± 0.3	1.87 ± 0.11	1,733.8 ± 795.4

Data are the mean ± S.D., $n = 3$.

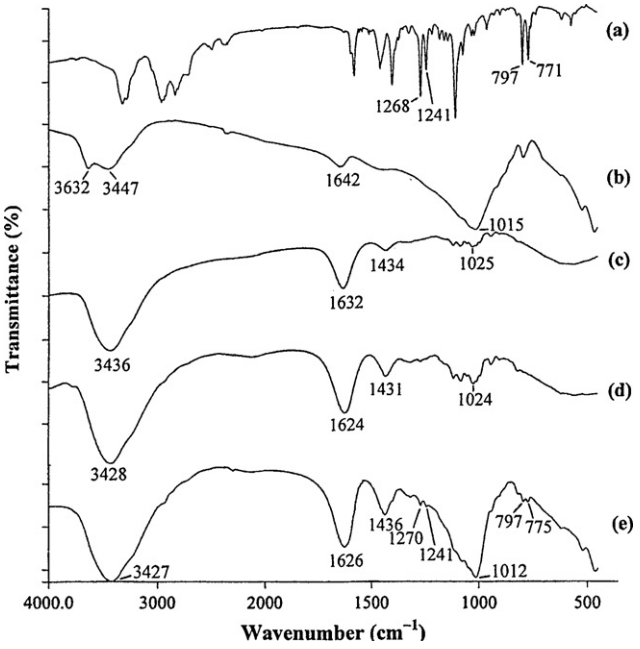

Fig. 2. FTIR spectra of PPN powder (a), MAS powder (b), blank CA beads (c), PPN-loaded CA beads (d), and PPN–1.5% MAS complex-loaded CA beads (e).

3.3. Thermal behavior

The thermal behavior of the CA beads was characterized using DSC, as shown in Fig. 3. SA powder presented two decomposition peaks at 258 and 351 °C (Fig. 3c). The blank CA beads presented a broad endothermic peak at 70 °C, and the exothermic peak of SA at 258 °C was absent (Fig. 3d). However, the second exothermic peak of the CA beads moved to a higher temperature (401 °C), indicating that the interaction of SA and calcium could enhance the thermal stability of SA. The interaction of PPN and SA caused a decrease in the thermal stability of the CA beads, evidenced by the shift of the exothermic peak to a lower temperature (Fig. 3e). The presence of MAS in the PPN-loaded CA beads caused an increase in the exothermic peak temperature (Fig. 3f and 3g). Moreover, an increasing MAS content lowered the intensity of the exothermic peak, and this peak was absent when 1.5% MAS was used (Fig. 3f–h). These data suggested that MAS could improve the thermal stability of the CA beads. Additionally, the DSC thermograms of the PPN- and PPN–MAS complex-loaded CA beads did not contain the melting peak of PPN at 164 °C (Fig. 3b), suggesting that PPN was molecularly dispersed in the MAS silicate layers and the CA bead matrix.

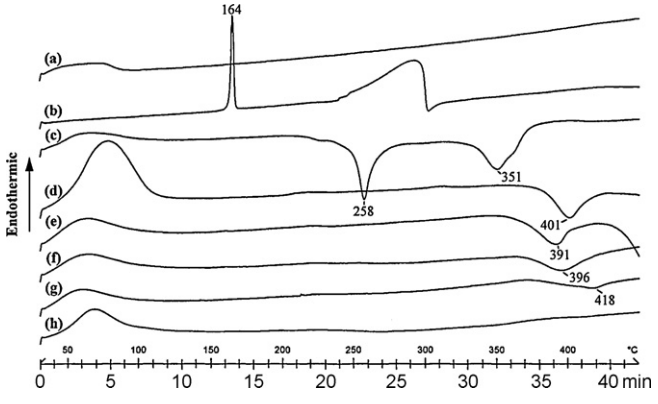

Fig. 3. FTIR spectra of MAS powder (a), PPN powder (b), SA powder (c), blank CA beads (d), PPN-loaded CA beads (e), and CA beads containing PPN–MAS complexes prepared using 0.38 (f), 0.75 (g), and 1.5 (h) % MAS.

3.4. Particle size and morphology

The mean particle size of all the beads prepared ranged from 1.07 to 1.28 mm and tended to increase with increasing content of MAS. The CA beads were spherical and are shown in the SEM photographs in Fig. 4. The PPN-loaded CA beads showed small white crystals throughout their surface and internal matrix (Fig. 4a and b, respectively). In contrast, many dark circle regions on the surface and in the matrix structure were observed in the PPN–1.5% MAS complex-loaded CA beads (Fig. 4c and d, respectively). EDX analysis was used to identify the main element of the dark circle regions in these beads. The results revealed that this region showed an element pattern of Mg, Al, and Si (Fig. 5b), which was obviously different than the pattern on the outside of this region (Fig. 5a). This finding indicated that the dark regions on the surface and in the matrix structure of the beads represented the PPN–MAS complexes. Furthermore, this finding suggested that the PPN–MAS complex-loaded CA beads were successfully prepared and the complexes, which were embedded in the beads, could possibly act as drug microreservoirs.

The presentation model of the PPN–MAS complex-loaded CA beads is illustrated in Fig. 6. The CA beads consisted of the PPN–MAS complex particles and the PPN molecules dispersed in the matrix. MAS has a layered structure that is constructed from tetrahedrally coordinated silica atoms fused into an edge-shared octahedral plane of either aluminum hydroxide or magnesium hydroxide. The PPN–MAS complexes were formed via cation exchange, hydrogen bonding, and water bridging interactions, allowing the PPN molecules to intercalate into the MAS silicate layers (Rojtanatanya & Pongjanyakul, 2010). Hence, this system is referred to as PPN–MAS intercalated complex-loaded CA beads.

3.5. Drug entrapment efficiency

The effect of the concentration of MAS on the ability of beads prepared using 2% calcium chloride to efficiency entrap PPN is shown in Fig. 7a. The drug entrapment efficiency of the beads significantly increased with increasing amounts of MAS. This observation indicated that the PPN–MAS complexes formed in the dispersion prior to cross-linking could enhance the drug entrapment efficiency of the beads. Increasing the concentration of MAS in the dispersions increased the amount of PPN adsorbed onto the MAS, resulting in higher drug entrapment efficiency. Moreover, the interaction of MAS with SA increased the barrier preventing water from leaking from the beads during the preparation period (Puttipipatkhachorn et al., 2005). This also could account for the reduction of drug lost from the beads.

The PPN entrapment efficiency was also affected when beads were formed with different concentrations of calcium chloride. Increases in calcium chloride concentration resulted in decreased drug entrapment efficiency of the PPN-loaded and the PPN–1.5% MAS complex-loaded CA beads (Fig. 7b). It is possible that enhanced bead shrinkage occurred during gelation under conditions with higher concentrations of calcium chloride (Østberg & Graffner, 1994). This shrinkage could have lead to a shorter path length for drug leakage, and therefore higher drug loss. Moreover, the calcium ions could have exchanged with PPN in the PPN–MAS complexes of the gel beads in a calcium concentration dependent manner. As a result, the PPN–1.5% MAS complex-loaded CA beads showed a greater decrease in drug entrapment efficiency when compared with the PPN-loaded CA beads. These results showed that the PPN–MAS complex-loaded CA beads provided remarkably higher drug entrapment efficiency due to the

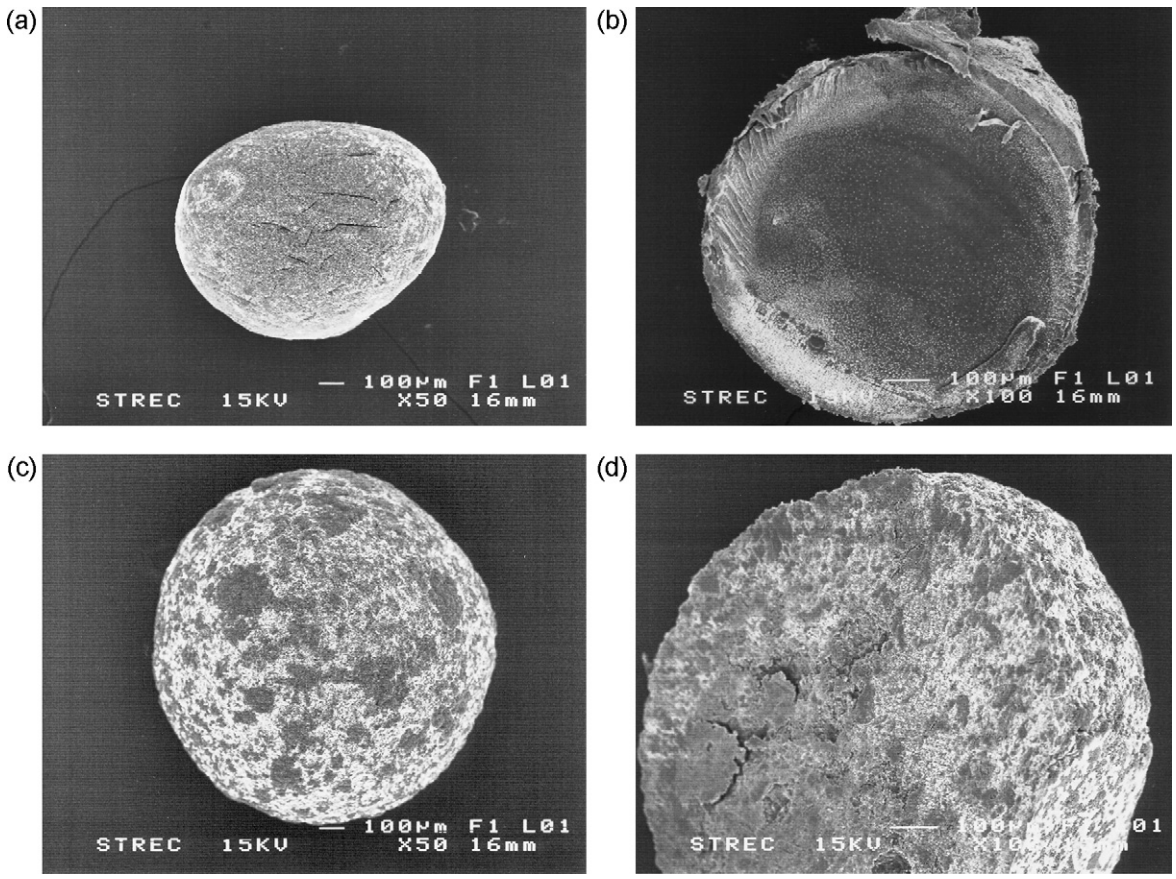

Fig. 4. Microscopic morphology and internal structure of PPN-loaded CA beads (a, b) and PPN–1.5% MAS complex-loaded CA beads (c, d) prepared using 2% calcium chloride.

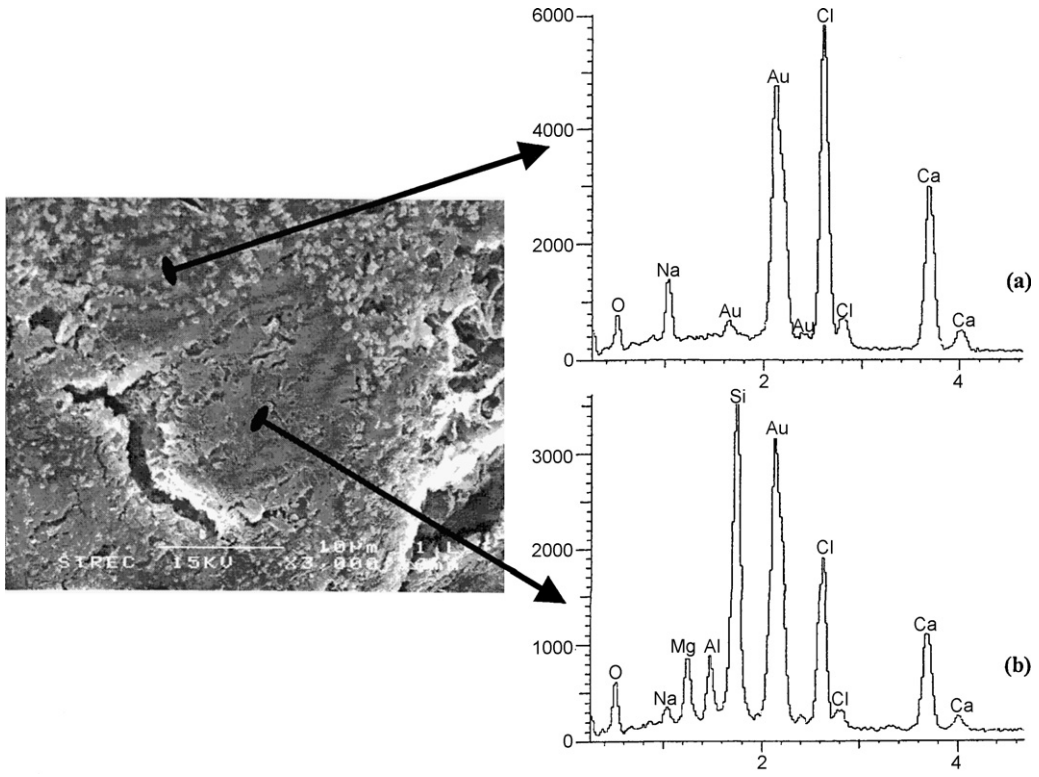

Fig. 5. SEM micrograph focused on PPN–MAS complexes in PPN–1.5% MAS complex-loaded CA beads and EDX patterns of CA matrix (a) and PPN–MAS complexes (b).

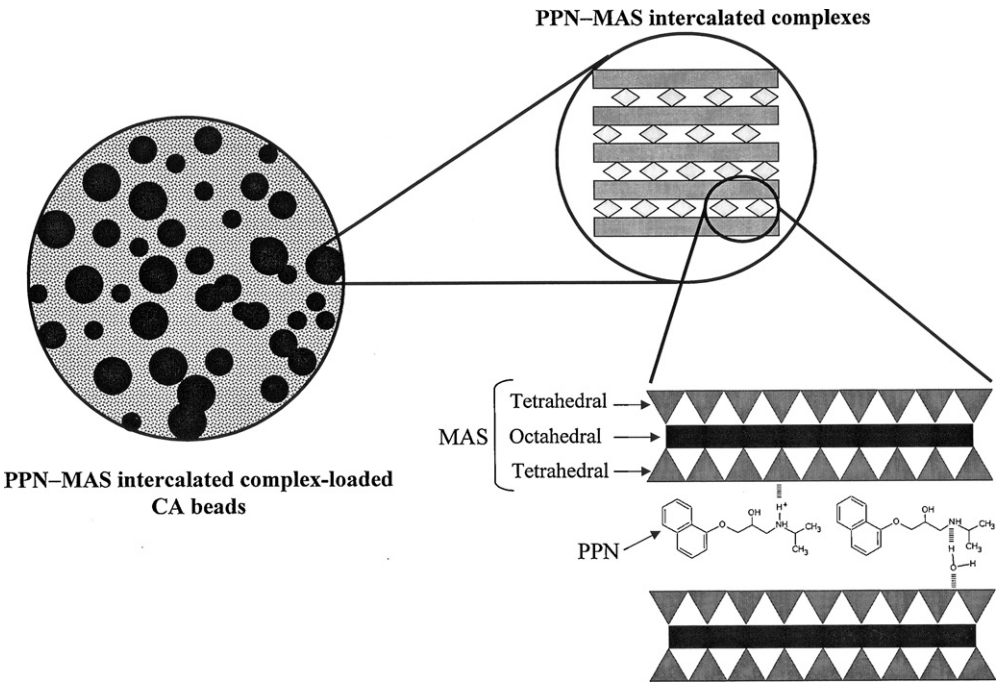

Fig. 6. Schematic presentation of PPN–MAS intercalated complex-loaded CA beads.

presence of the PPN–MAS complexes, which act as drug micro-reservoirs.

3.6. Mechanical property

The maximum force for 50% displacement was used to evaluate the strength of the CA beads. The effect of MAS on the strength of the beads using 2% calcium chloride is shown in Fig. 8a. The maximum force for 50% displacement of the PPN-loaded beads gradually increased with increasing MAS content. This result indicated that the interaction of SA and MAS could create a dense matrix structure that reinforced the strength of the CA beads. In addition, the PPN–1.5% MAS complex-loaded CA beads were weaker when tested under conditions of increasing calcium chloride concentration (Fig. 8b). It is probable that the higher concentration of calcium chloride could rapidly cross-link with the denser network of CA on the surface of the gel beads, leading to the slower diffusion of calcium ions into the interior of the beads during the cross-linking process. Moreover, a limited duration of time (30 min) for the cross-linking process was used in this study. Thus, under high concentrations of calcium chloride, incomplete cross-linking in the interior of the beads may have occurred, resulting in the decreased strength of the beads.

3.7. In vitro drug release

The PPN release profiles of the CA beads containing PPN–MAS complexes prepared using various MAS concentrations in 0.1 M HCl and pH 6.8 phosphate buffer are shown in Fig. 9. The PPN-loaded CA beads gave the highest initial burst of drug release at 5 min and complete drug release in both media tested (Table 2). The initial burst of drug release of these beads in an acidic medium was higher than the same beads in pH 6.8 phosphate buffer. In addition, the initial burst release of the beads significantly decreased with increasing MAS content (Table 2). The release of PPN from the CA beads in 0.1 M HCl showed a strong correlation with the square root of time ($R^2 > 0.95$), indicative of a matrix diffusion controlled mechanism. In contrast, in the pH 6.8 phosphate buffer, the drug release displayed a good fit with respect to time ($R^2 > 0.95$), suggesting zero order release kinetics. These data indicated PPN release was dependent on a polymer swelling mechanism. The rate of release and the amount of PPN released at 10 h in both media are listed in Table 2. Both PPN release parameters obviously decreased with increasing MAS content. Moreover, a higher amount of PPN was released at 10 h in 0.1 M HCl, as compared to the amount released using pH 6.8 phosphate buffer.

The release of PPN from the PPN- and the PPN–MAS complex-loaded CA beads in 0.1 M HCl and pH 6.8 phosphate buffer revealed different release mechanisms and that were influenced by the type of cation present in the release medium. It is probable that the calcium ions in the CA beads were totally exchanged with hydrogen ions in the acidic medium, which lead to a unionized form of the carboxyl groups of SA. This could have led to the formation of an insoluble alginic matrix bead for sustained drug release, and therefore the drug release can be explained by a matrix diffusion controlled mechanism. Alternatively, the CA beads could have swelled in a sodium ion-rich medium (pH 6.8 phosphate buffer). The swelling of the CA matrices would have occurred via an exchange of cross-linking calcium ions with sodium ions (Østberg et al., 1994). Thus, the partial formation of soluble SA occurred. In addition, CA gels could be solubilized in the medium containing phosphate ions, which acted as a calcium ion complexing agent at pH levels above 5.5 (Remuñán-López & Bodmeier, 1997). For these reasons, the CA beads had higher water uptake and demonstrated swelling properties in the pH 6.8 phosphate buffer. Thus, the PPN release was controlled by swelling of the beads (Pongjanyakul & Puttipipatkhachorn, 2007a; Puttipipatkhachorn et al., 2005).

The initial burst release of PPN in the PPN-loaded CA beads was significantly decreased when increased MAS content was used, suggesting that the PPN–MAS complexes formed prior to cross-linking to the CA beads could control drug release and reduce drug leaching from the CA beads. However, the initial burst release in the acidic medium was higher than the release in pH 6.8 phosphate buffer. This was due to a faster PPN release of the PPN–MAS complexes in 0.1 M HCl when compared to the pH 6.8 phosphate buffer

Table 2
PPN release characteristics of PPN–MAS complex-loaded CA beads.

PPN-loaded CA beads	0.1 M HCl			pH 6.8 phosphate buffer		
	Initial burst release at 5 min (%)	Release rate (% $min^{-1/2}$)	PPN released at 10 h (%)	Initial burst release at 5 min (%)	Release rate (% min^{-1})	PPN released at 10 h (%)
Effect of MAS						
−0% (w/v) MAS	86.2 ± 1.9	–	103.9 ± 2.8	62.2 ± 8.2	–	103.8 ± 2.4
−0.38% (w/v) MAS	42.2 ± 0.9	14.05 ± 0.05 (R^2 = 0.952)	89.8 ± 0.7	15.5 ± 1.2	0.77 ± 0.02 (R^2 = 0.955)	82.4 ± 2.5
−0.75% (w/v) MAS	23.4 ± 1.2	8.64 ± 0.08 (R^2 = 0.982)	73.8 ± 1.1	8.41 ± 0.70	0.34 ± 0.02 (R^2 = 0.997)	67.8 ± 0.2
−1.50% (w/v) MAS	10.7 ± 0.7	2.88 ± 0.02 (R^2 = 0.979)	51.1 ± 0.5	2.65 ± 1.05	0.22 ± 0.01 (R^2 = 0.987)	46.2 ± 0.6
Effect of $CaCl_2$						
−0.5% (w/v) $CaCl_2$	9.66 ± 0.54	3.33 ± 0.05 (R^2 = 0.997)	54.3 ± 1.4	0.39 ± 0.57	0.17 ± 0.01 (R^2 = 0.988)	56.0 ± 3.4
−1.0% (w/v) $CaCl_2$	11.1 ± 1.5	2.82 ± 0.09 (R^2 = 0.995)	50.3 ± 1.1	1.95 ± 1.09	0.14 ± 0.01 (R^2 = 0.982)	48.8 ± 0.3
−2.0% (w/v) $CaCl_2$	10.7 ± 0.7	2.88 ± 0.02 (R^2 = 0.979)	51.1 ± 0.5	2.65 ± 1.05	0.22 ± 0.01 (R^2 = 0.987)	46.2 ± 0.6

Data are the mean ± S.D., n = 3.

(Rojtanatanya & Pongjanyakul, 2010). Moreover, the gel formation and swelling property of the CA beads in pH 6.8 phosphate buffer could retard initial drug release, resulting in the lower burst release observed in the pH 6.8 phosphate buffer solution. After the initial stage of drug release, the PPN release rate also decreased as a function of the amount of MAS. In the case of the acidic medium, the MAS could have interacted with SA before the cross-linking process, which could reinforce the matrix structure of the CA beads, despite the fact that the beads were exposed in an acidic medium. Increases in the MAS content in the beads, resulted in denser matrix structures. Furthermore, increases in MAS content resulted in greater particle sizes of PPN–MAS complexes in the CA beads (Table 1). Additionally, the presence of MAS in the CA beads did not affect water uptake but obviously reduced the swelling capability of the CA beads in the pH 6.8 phosphate buffer (Puttipipatkhachorn et al., 2005). These results revealed the rate of drug release of the

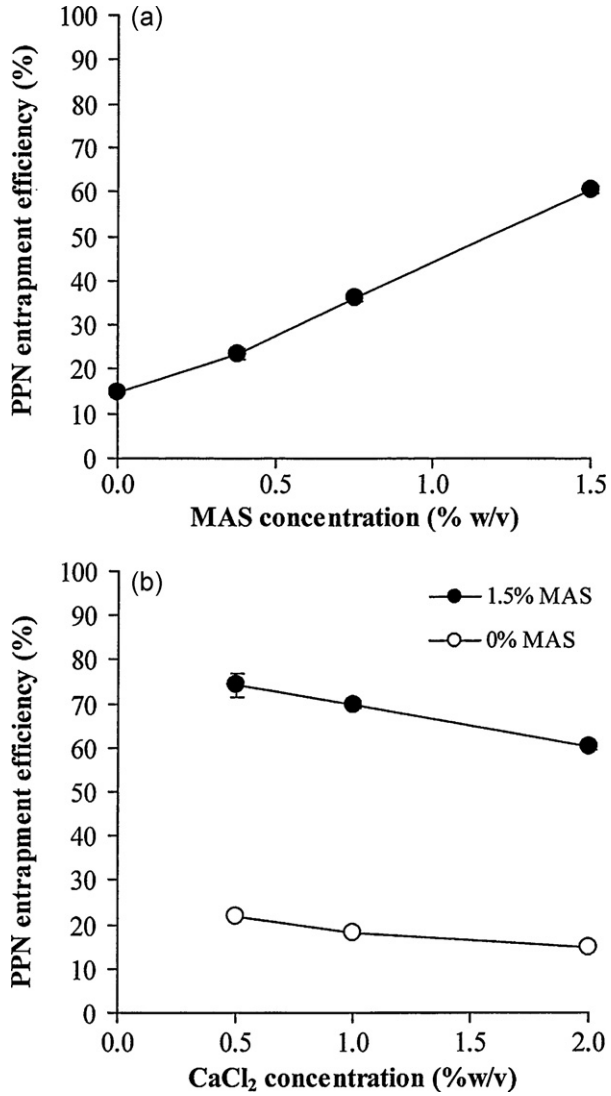

Fig. 7. Effect of MAS (a) and calcium chloride concentrations used (b) on PPN entrapment efficiency of CA beads. Each point is the mean ± S.D., n = 3.

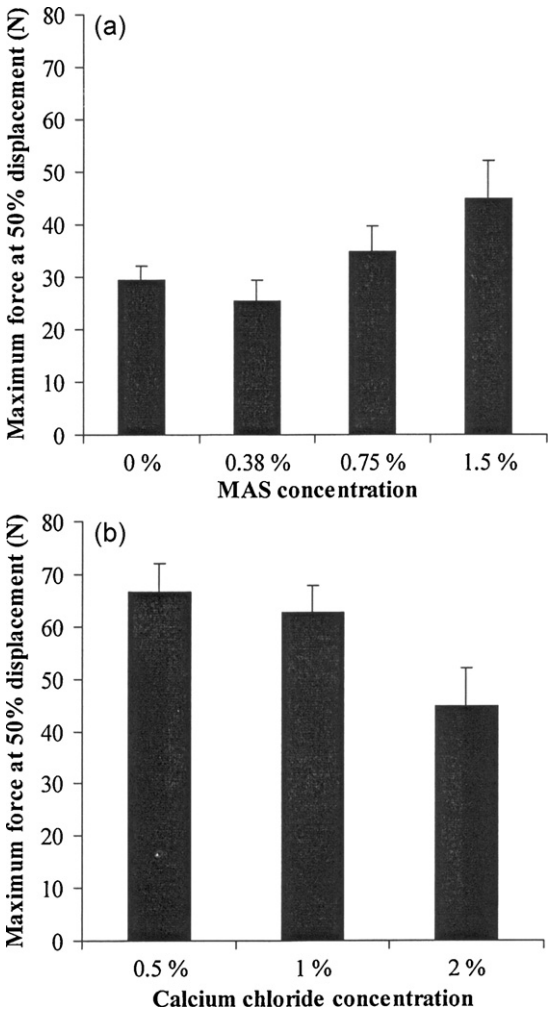

Fig. 8. Effect of MAS (a) and calcium chloride (b) concentrations used on mechanical properties of PPN–MAS complex-loaded CA beads. Each value is the mean ± S.D., n = 10.

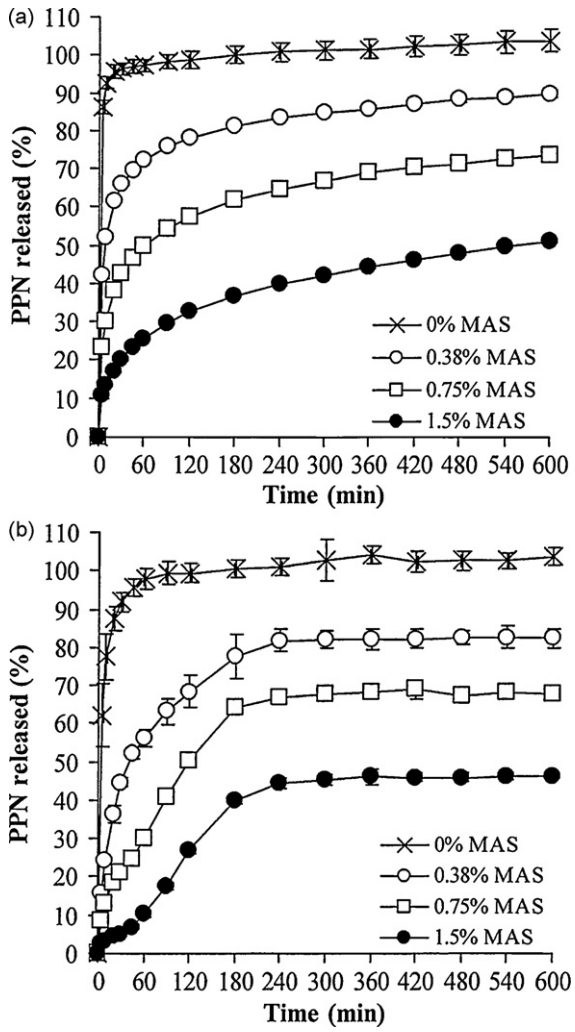

Fig. 9. PPN release profiles of CA beads containing PPN–MAS complexes prepared using different MAS concentrations in 0.1 M HCl (a) and pH 6.8 phosphate buffer (b). Each point is the mean ± S.D., $n = 3$.

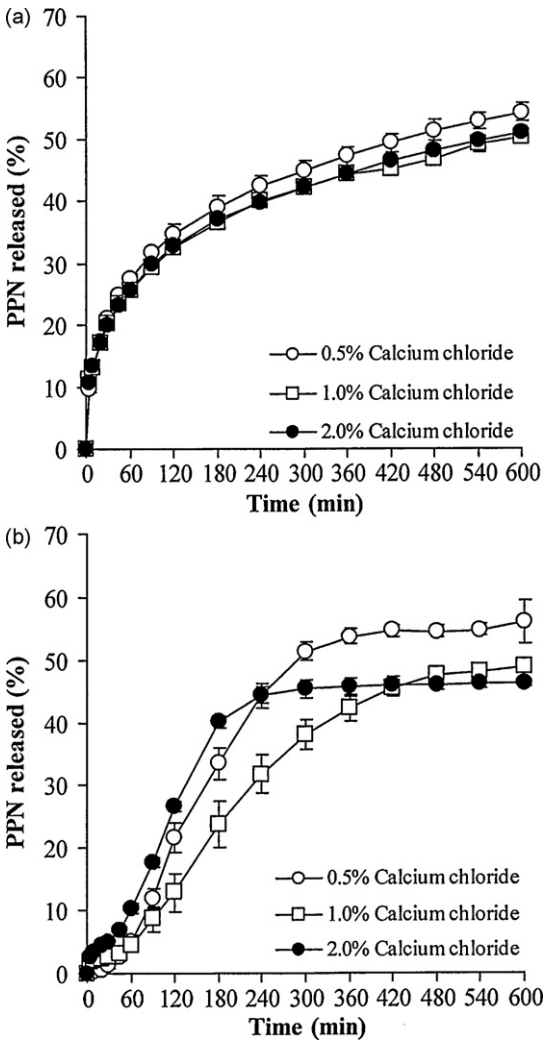

Fig. 10. PPN release profiles of PPN–1.5% MAS complex-loaded CA beads prepared using different calcium chloride concentrations in 0.1 M HCl (a) and pH 6.8 phosphate buffer (b). Each point is the mean ± S.D., $n = 3$.

PPN–MAS complex-loaded CA beads decreased when higher MAS content was used.

The last drug release parameter of the PPN- and the PPN–MAS complex-loaded CA beads was the amount of PPN released at 10 h. Complete PPN release was found only for the PPN-loaded CA beads in either release media. The PPN released at 10 h of the PPN–MAS complex-loaded CA beads in 0.1 M HCl was higher than the release in pH 6.8 phosphate buffer, and this release parameter also decreased with increasing MAS content in the beads. The higher percentage of PPN release from the PPN–MAS complexes in acidic medium was because the PPN–MAS complexes were embedded in the bead matrix (Rojtanatanya & Pongjanyakul, 2010). The higher MAS content in the beads provided a greater affinity for PPN, resulting in a lower amount of PPN released at 10 h. Recently, many researchers have reported that drug–clay complexes provide incomplete drug release (Joshi, Kevadiya, Patel, Bajaj, & Jasra, 2009; Jung, Kim, Choy, Hwang, & Choy, 2008; Park et al., 2008). This release behavior was also characteristic of alginate films containing drug–clay complexes (Pongjanyakul & Suksri, 2009). Jung et al. (2008) described that it is difficult for cations in the solution to exchange with drug molecules inside the MAS layers. This ion exchange process may result in zipping of the crystal edge and a shortening of the distance between the layers. However, these reports revealed that the ion exchange process between the complexes and counter ions in the surrounding medium could reach an equilibrium of drug release, which is similar to the drug release behavior of drug-synthetic ion exchange resin complexes (Borodkin, 1993).

The effect of the concentration of calcium on the release of PPN from the PPN–1.5% MAS complex-loaded CA beads was also investigated and results are shown in Fig. 10. The increase in calcium concentration for cross-linking did not influence the release profiles and parameters of PPN when using 0.1 M HCl as the media (Fig. 10 and Table 2). These results are in agreement with a previous study by Østberg and Graffner (1994). These data suggested the formation of the insoluble alginic matrix bead occurred rapidly and a similar matrix structure was obtained. Combined these effects could have lead to the similar release rates of PPN observed. In contrast, in experiments using pH 6.8 phosphate buffer, the initial burst release of the beads tended to increase with increasing calcium chloride concentration (Table 2). This is possibly because the drug molecules, which can leach out the wet beads during the gelation process, may have accumulated at the surface of the wet beads. Denser cross-linking at the surface of the beads occurred when higher concentrations of calcium chloride were used. The rate of PPN release from the beads decreased with increasing calcium chloride concentration from 0.5 to 1% (w/v). However, an increase in the rate of drug release was found when using 2% calcium chloride. This

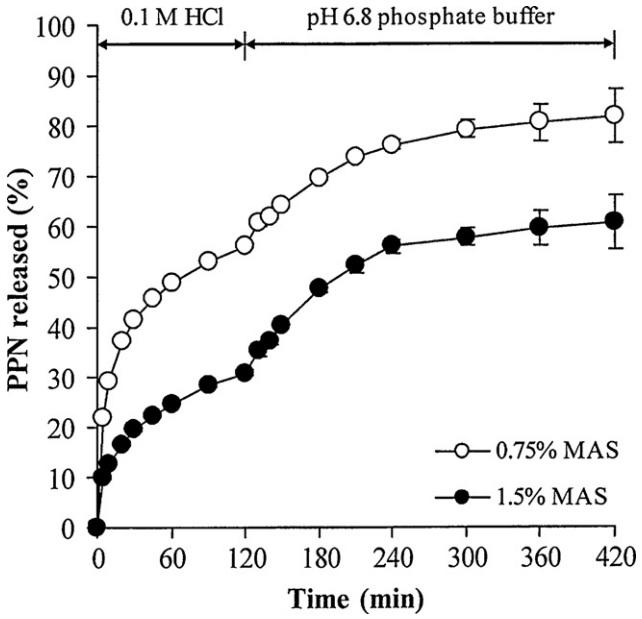

Fig. 11. PPN release profiles of CA beads containing PPN–MAS complexes prepared using 0.75 and 1.5% MAS in simulated gastro-intestinal condition. Each point is the mean ± S.D., $n = 3$.

result suggested that exposing the beads to 2% calcium chloride after treatment with pH 6.8 phosphate buffer increased swelling due to incomplete cross-linking in the interior of the beads. Results demonstrating the decreased strength of the beads support this hypothesis (Fig. 8b). These conditions released the greatest amount of drug.

Due to the fact that PPN was incompletely released in either 0.1 M HCl or pH 6.8 phosphate buffer, simulated gastro-intestinal conditions starting with 0.1 M HCl for 2 h followed by pH 6.8 phosphate buffer were used to investigate the amount of PPN released from the PPN–MAS complex-loaded CA beads. The release of PPN from the CA beads containing PPN–MAS complexes prepared using 0.75 and 1.5% MAS proceeded continuously when the dissolution medium was changed from acidic medium to pH 6.8 phosphate buffer (Fig. 11). The swollen beads could be visualized when the release medium was changed to pH 6.8 phosphate buffer. This indicated that the alginic matrix beads formed in the acidic medium could convert to SA allowing the sodium ions in the phosphate buffer to exchange with drug in the PPN–MAS complexes, leading to higher amount of PPN release when compared with either 0.1 M HCl or pH 6.8 phosphate buffer. This finding suggested that the release of PPN could possibly take place continuously when the PPN–MAS complex-loaded CA beads were transferred from the stomach to the small intestine in the GI tract.

4. Conclusions

This study demonstrated that the molecular interaction of MAS with PPN and SA resulted in PPN–MAS intercalated complex particles and denser matrix structure formation in the CA beads. The PPN–MAS intercalated complexes formation enhanced PPN entrapment efficiency and modulated PPN release in both acidic medium and pH 6.8 phosphate buffer. The PPN entrapment efficiency of the PPN–MAS complex-loaded CA beads was remarkably higher than that of the PPN-loaded CA beads. Increasing the MAS content of these beads resulted in an increase in PPN entrapment efficiency, thermal stability, and strength of the CA beads. Moreover, the initial burst of PPN and its rate of release were decreased in the PPN–MAS complex-loaded CA beads, which was dependent on the MAS content added. Additionally, the PPN–MAS complex-loaded CA beads also demonstrated a sustained release pattern of PPN in the simulated GI conditions. These results suggested that the CA beads containing drug–clay intercalated complexes, which served as microreservoirs, showed strong potential as an oral drug delivery system for cationic drugs with high water solubility.

Acknowledgments

The authors would like to thank the Thailand Research Fund (Bangkok, Thailand) for research funding (Grant No. RSA5280013). We are very pleased to acknowledge the Center for Research and Development of Herbal Health Products and the Faculty of Pharmaceutical Sciences, Khon Kaen University (Khon Kaen, Thailand), for technical support.

References

Almeida, P. F., & Almeida, A. J. (2004). Cross-linked alginate-gelatin beads: A new matrix for controlled release of pindolol. *Journal of Controlled Release*, *97*, 431–439.
Bechgaard, H., & Nielsen, G. H. (1978). Controlled-release multiple-units and single-unit doses. *Drug Development and Industrial Pharmacy*, *4*, 53–67.
Bertram, U., & Bodmeier, R. (2006). In situ gelling, bioadhesive nasal inserts for extended drug delivery: In vitro charaterization of a new nasal dosage form. *European Journal of Pharmaceutical Sciences*, *27*, 62–71.
Borodkin, P. B. (1993). Ion exchange resins and sustained release. In J. Swarbrick, & J. C. Boylan (Eds.), *Encyclopedia of pharmaceutical technology* (pp. 203–216). New York: Marcel Dekker, Inc.
Costa, P., & Lobo, J. M. S. (2001). Modeling and comparison of dissolution profiles. *European Journal of Pharmaceutical Sciences*, *13*, 123–133.
Dollery, S. C. (1991). *Therapeutic drugs*. Edinburgh: Churchill Livingstone.
Draget, K. I. (2000). Alginates. In G. O. Philips, & P. A. Williams (Eds.), *Handbook of hydrocolloids* (pp. 379–395). Cambridge: Woodhead Publishing.
Edwards-Lévy, F., & Lévy, M. C. (1999). Serum albumin–alginate coated beads: Mechanical properties and stability. *Biomaterials*, *20*, 2069–2084.
Fernández-Hervás, M. J., Holgado, M. A., Fini, A., & Fell, J. T. (1998). In vitro evaluation of alginate beads of a diclofenac salt. *International Journal of Pharmaceutics*, *163*, 23–34.
Grant, G. T., Morris, E. R., Rees, D. A., Smith, P. J. C., & Thom, D. (1973). Biological interaction between polysaccharides and divalent cations: The egg-box model. *FEBS Letters*, *32*, 195–198.
Gupta, M. K., Vanwert, A., & Bogner, R. H. (2003). Formation of physical stable amorphous drugs by milling with Neusilin. *Journal of Pharmaceutical Sciences*, *92*, 536–551.
Halder, A., Maiti, S., & Sa, B. (2005). Entrapment efficiency and release characteristics of polyethyleneimine-treated or -untreated calcium alginate beads loaded with propranolol–resin complex. *International Journal of Pharmaceutics*, *302*, 84–94.
Hwang, S. J., Rhee, G. J., Lee, K. M., Oh, K. H., & Kim, C. K. (1995). Release characteristics of ibuprofen from excipient-loaded alginate gel beads. *International Journal of Pharmaceutics*, *116*, 125–128.
Joshi, G. V., Kevadiya, B. D., Patel, H. A., Bajaj, H. C., & Jasra, R. V. (2009). Montmorillonite as a drug delivery system: Intercalation and in vitro release of timolol maleate. *International Journal of Pharmaceutics*, *374*, 53–57.
Jung, H., Kim, H., Choy, Y. B., Hwang, S., & Choy, J. (2008). Itraconazole-laponite: Kinetics and mechanism of drug release. *Applied Clay Science*, *40*, 99–107.
Kibbe, H. A. (2000). *Handbook of pharmaceutical excipients*. Washington: American Pharmaceutical Association.
Lee, B. J., Min, G. H., & Cui, J. H. (1999). Correlation of drug solubility with trapping efficiency and release characteristics of alginate beads. *Pharmacy and Pharmacology Communications*, *5*, 85–89.
Lim, L. Y., & Wan, L. S. C. (1997). Propranolol hydrochloride binding in calcium alginate beads. *Drug Development and Industrial Pharmacy*, *23*, 973–980.
Martin, A. (1993). *Physical pharmacy*. Philadelphia: Lea & Febiger.
Murata, Y., Miyamoto, E., & Kawashima, S. (1996). Additive effect of chondroitin sulfate and chitosan on drug release from calcium-induced alginate gel beads. *Journal of Controlled Release*, *38*, 101–108.
Murata, Y., Tsumoto, K., Kofuji, K., & Kawashima, S. (2003). Effect of natural polysaccharide addition on drug release from calcium-induced alginate gel beads. *Chemical and Pharmaceutical Bulletin*, *51*, 218–220.
Østberg, T., & Graffner, C. (1994). Calcium alginate matrices for oral multiple unit administration. III. Influence of calcium concentration, amount of drug added and alginate charateristics on drug release. *International Journal of Pharmaceutics*, *111*, 271–282.
Østberg, T., Lund, E. M., & Graffner, C. (1994). Calcium alginate matrices for oral multiple unit administration. IV. Release characteristics in different media. *International Journal of Pharmaceutics*, *112*, 241–248.
Paker-Leggs, S., & Neau, S. H. (2009). Pellet characteristics and drug release when the form of propranolol is fixed as moles or mass in formulations for extruded and spheronized Carbopol-containing pellets. *International Journal of Pharmaceutics*, *369*, 96–104.

Park, J. K., Choy, Y. B., Oh, J., Kim, J. Y., Hwang, S., & Choy, J. (2008). Controlled release of donepezil intercalated in smectite clays. *International Journal of Pharmaceutics*, *359*, 198–204.

Pongjanyakul, T., Khunawattanakul, W., & Puttipipatkhachorn, S. (2009). Physicochemical characterizations and release studies of nicotine-magnesium aluminum silicate complexes. *Applied Clay Science*, *44*, 242–250.

Pongjanyakul, T., & Puttipipatkhachorn, S. (2007a). Xanthan–alginate composite gel beads: Molecular interaction and in vitro characterization. *International Journal of Pharmaceutics*, *331*, 61–71.

Pongjanyakul, T., & Puttipipatkhachorn, S. (2007b). Sodium alginate-magnesium aluminum silicate composite gels: Characterization of flow behavior, microviscosity, and drug diffusivity. *AAPS PharmSciTech*, *8*, E72.

Pongjanyakul, T., & Suksri, H. (2009). Alginate-magnesium aluminum silicate films for buccal delivery of nicotine. *Colloids and Surfaces B: Biointerfaces*, *74*, 103–113.

Puttipipatkhachorn, S., Pongjanyakul, T., & Priprem, A. (2005). Molecular interaction in alginate beads reinforced with sodium starch glycolate or magnesium aluminum silicate, and their physical characteristics. *International Journal of Pharmaceutics*, *293*, 51–62.

Remuñán-López, C., & Bodmeier, R. (1997). Mechanical, water uptake and permeability properties of crosslinked chitosan glutamate and alginate films. *Journal of Controlled Release*, *44*, 215–225.

Rojtanatanya, S., & Pongjanyakul, T. (2010). Propranolol–magnesium aluminum silicate complex dispersions and particles: Characterization and factors influencing drug release. *International Journal of Pharmaceutics*, *383*, 106–115.

Sartori, C., Finch, D. S., & Ralph, B. (1997). Determination of the cation content of alginate thin films by FTIR spectroscopy. *Polymer*, *38*, 43–51.

Sugawara, S., Imai, T., & Otagiri, M. (1994). The controlled release of prednisolone using alginate gel. *Pharmaceutical Research*, *11*, 272–277.

Suksri, H., & Pongjanyakul, T. (2008). Interaction of nicotine with magnesium aluminum silicate at different pHs: Characterization of flocculate size, zeta potential and nicotine adsorption behavior. *Colloids and Surfaces B: Biointerfaces*, *65*, 54–60.

Takada, K., & Yoshikawa, H. (1999). Oral drug delivery, traditional. In E. Mathiowitz (Ed.), *Encyclopedia of controlled drug delivery* (pp. 728–742). New York: John Wiley & Sons, Inc.

Viseras, C., Aguzzi, C., Cerezo, P., & Lopez-Galindo, A. (2007). Uses of clay minerals in semisolid health care and therapeutic products. *Applied Clay Science*, *36*, 37–50.

Wang, K., & He, Z. (2002). Alginate-konjac glucomannan-chitosan beads as controlled release matrix. *International Journal of Pharmaceutics*, *244*, 117–126.